SCIENCE CHINA
Chemistry

•REVIEWS•

February 2021 Vol.64 No.2: 204–217
https://doi.org/10.1007/s11426-020-9869-4

# Designed fabrication of mesoporous silica-templated self-assembled theranostic nanomedicines

Yang Du[1,4,5], Zheng Chen[1], Ji Young Lee[1], Peihua Lin[1], Fan Xia[1], Yunan Guan[1], Fangyuan Li[1] & Daishun Ling[1,2,3*]

[1]*Institute of Pharmaceutics, College of Pharmaceutical Sciences, Zhejiang University, Hangzhou 310058, China;*
[2]*Key Laboratory of Biomedical Engineering of the Ministry of Education, College of Biomedical Engineering & Instrument Science, Zhejiang University, Hangzhou 310027, China;*
[3]*Hangzhou Institute of Innovative Medicine, College of Pharmaceutical Sciences, Zhejiang University, Hangzhou 310058, China;*
[4]*Department of Hepatobiliary and Pancreatic Surgery, The Second Affiliated Hospital, Zhejiang University School of Medicine, Hangzhou 310009, China;*
[5]*Key Laboratory of Precision Diagnosis and Treatment for Hepatobiliary and Pancreatic Tumor of Zhejiang Province, Hangzhou 310009, China*

Received August 17, 2020; accepted September 7, 2020; published online December 1, 2020

Theranostic nanosystems that integrate diagnosis and therapy have garnered increasing attention for personalized medicine. The integration of the versatile nanoparticles to fabricate self-assembled theranostic nanomedicines becomes increasingly important in current medical research. Mesoporous silica nanoparticles (MSN) with their highly attractive physicochemical properties and favorable morphological attributes represent ideal templates for the controlled assembly and integration of functional nanomaterials to fabricate self-assembled theranostic nanomedicines. The rationally designed combination strategy and heterostructure will improve the overall bioavailability and preserve the unique property of each nanocomponent. In this review, the cutting-edge strategies for the designed fabrication of MSN-templated self-assembled nanomedicines are summarized. We categorize MSN-based nanomedicines by their unique heterostructures, including core-shell, yolk-shell, core-satellite, heterodimer and core-shell-satellite structures, and discuss the controlled assembly approaches as well as the intriguing applications for disease theranostics. Finally, a perspective on the challenges in the clinical translation of self-assembled theranostic nanomedicines is highlighted.

**self-assembly, theranostics, heterostructure, mesoporous silica, nanomedicines**

**Citation:** Du Y, Chen Z, Lee JY, Lin P, Xia F, Guan Y, Li F, Ling D. Designed fabrication of mesoporous silica-templated self-assembled theranostic nanomedicines. *Sci China Chem*, 2021, 64: 204–217, https://doi.org/10.1007/s11426-020-9869-4

## 1 Introduction

The past decades have witnessed significant nanotechnological advances in biomedical applications [1]. The functional nanomaterials with unique electrical, thermal, optical, catalytic and magnetic properties are extensively used to serve as drug delivery vehicles, imaging probes as well as therapeutic agents for efficient medical diagnosis, monitoring and treatment of diseases [1–3]. For example, doxorubicin (DOX)-loaded liposome, Doxil, the first US Food and Drug Administration (FDA)-approved nanomedicine has shown a therapeutic effect on ovarian cancer and multiple myeloma with reduced heart-related side effects [4]. Meanwhile, inorganic nanoparticles, such as iron oxide nanoparticles, can be used as magnetic resonance imaging (MRI) contrast agents for medical diagnosis [5]. Recently, self-assembled

*Corresponding author (email: lingds@zju.edu.cn)

© Science China Press and Springer-Verlag GmbH Germany, part of Springer Nature 2020

theranostic nanosystems with the multiple capabilities such as targeted drug delivery, imaging, and therapy, have received growing attention for personalized medicine [6]. Simultaneous employment of the therapeutic functions during the diagnostic procedures, so-called theranostics, may interfere and deter the disease development at an early stage for enhanced therapeutic efficacy [7,8]. Thus, the integration of the versatile nanoparticles to fabricate self-assembled theranostic nanomedicines becomes increasingly important in current medical research [9,10]. Among various nanoparticles, mesoporous silica nanoparticles (MSN) have been widely studied for the design of theranostic nanomedicines since the first biomedical application for drug delivery [11,12]. The synthesis of MSN with controlled shape and size, large surface area and tunable pore volume is readily available, and the easy modification of MSN makes it suitable for the controlled assembly of targeting moieties, diagnostic agents and therapeutic agents [13]. Compared with other porous nanomaterials, MSN have great advantages for cargo delivery due to their larger pore size than that of zeolites and better thermal and chemical stability as compared with metal-organic frameworks or covalent organic frameworks [14–16]. These overall advantages enable them to efficiently perform their functions under harsh biological conditions [17]. Moreover, silica is approved by the FDA in many food additives, which reveals its safety for potential clinical translation [18]. Recently, several comprehensive reviews on MSN have been published, most of them highlighted the functionalities of MSN as well as their applications in drug delivery and targeted therapy [19–22]. However, few of them focus on the assembly strategies using MSN as the templates to construct multifunctional nanomedicines for disease theranostics. In this review, the recent advances of MSN-templated self-assembled theranostic nanomedicines with diverse heterostructures are summarized, and their biomedical applications are intensively discussed.

## 2 Structures of MSN-templated self-assembled theranostic nanomedicines

Generally, MSN are synthesized by a surfactant mediated sol-gel reaction [23]. The surfactant such as cetyltrimethylammonium bromide (CTAB) serves as the micelle template for the hydrolysis and condensation of organosilane precursors under alkali condition [24]. The size, shape and pore volume of MSN could be rationally controlled by adjusting the ratio of silica precursors to solvent, the type of surfactants and pH values [25,26]. Functional nanocomponents can be incorporated into MSN during the synthetic procedure or be assembled on the surface of MSN *via* an appropriate post-synthesis modification [27]. Surface functionalization of MSN is needed to create active sites for the integration of functional nanocomponents. Silicane coupling agents, such as aminopropyltrimethoxysilane can introduce amine, thiol or carboxyl groups onto the surface and pores of the MSN matrix [28,29]. Consequently, functional nanocomponents can integrate into MSN *via* covalent/non-covalent linkage [30]. Moreover, functional molecules, such as PEG, antibody, organic dye, can be easily coupled with MSN for prolonged blood circulation time, enhanced targeting ability and imaging performance [31,32]. The diverse modifiability of MSN allows it to form different heterostructures by adopting different assembly methods. There are five common types for the formation of self-assembled theranostic nanomedicines, including core-shell, yolk-shell, core-satellite, heterodimer, and core-shell-satellite (Figure 1). The synthetic methods, structure properties, and applications of different MSN-templated self-assembled theranostic nanomedicines with various heterostructures are summarized in Table 1.

### 2.1 Core-Shell Structure

For core-shell structures, MSN shell is formed on the surface of functional nanoparticles. Generally, the surface modification is necessary for the growth of MSN shell. Therefore, surfactants such as CTAB are typically applied to transfer the functional nanoparticles from organic phase to water phase, and act as templates for the formation of silica shell *via* a sol-gel reaction (Figure 2(a)) [33]. Functional nanoparticles encapsulated inside silica shells can enhance their stability in physiological media, and preserve their unique properties for further biomedical applications [34]. Moreover, the MSN coating usually reduces the toxicity of the embedded functional nanoparticles, showing improved biocompatibility [35]. MSN coated iron oxide nanoparticles (IONPs) [36], gold nanoparticles (AuNPs) [37,38], upconversion nanoparticles (UCNPs) [39,40] and carbon nanotubes [41], with excellent optical, magnetic, magnetothermal or photothermal properties, are most commonly investigated for biomedical applications. For example, Liu and co-workers [42] coated UCNP ($NaYF_4$:$Yb^{3+}$/$Tm^{3+}$@$NaYF_4$) with MSN shell through a CTAC-assisted approach. The mesopores of as-synthesized UCNP@$mSiO_2$ were modified with azobenzene derivatives and further loaded with DOX. This core-shell structured nanomedicine realized NIR light-regulated precise drug release (Figure 2(b)). Hyeon group [36] developed a multifunctional monodisperse nanocomposite ($Fe_3O_4$@MSN) consisting of a single $Fe_3O_4$ nanocrystal core and an MSN shell (Figure 2(c)). The as-synthesized core-shell $Fe_3O_4$@MSN exhibited excellent tumor MR imaging. Non-spherical nanomaterials could also be loaded within MSN to form the core-shell structure. Zhang and co-workers [38] prepared MSN coated gold nanorods (Au@$SiO_2$) by the CTAB assisted sol-gel process, which

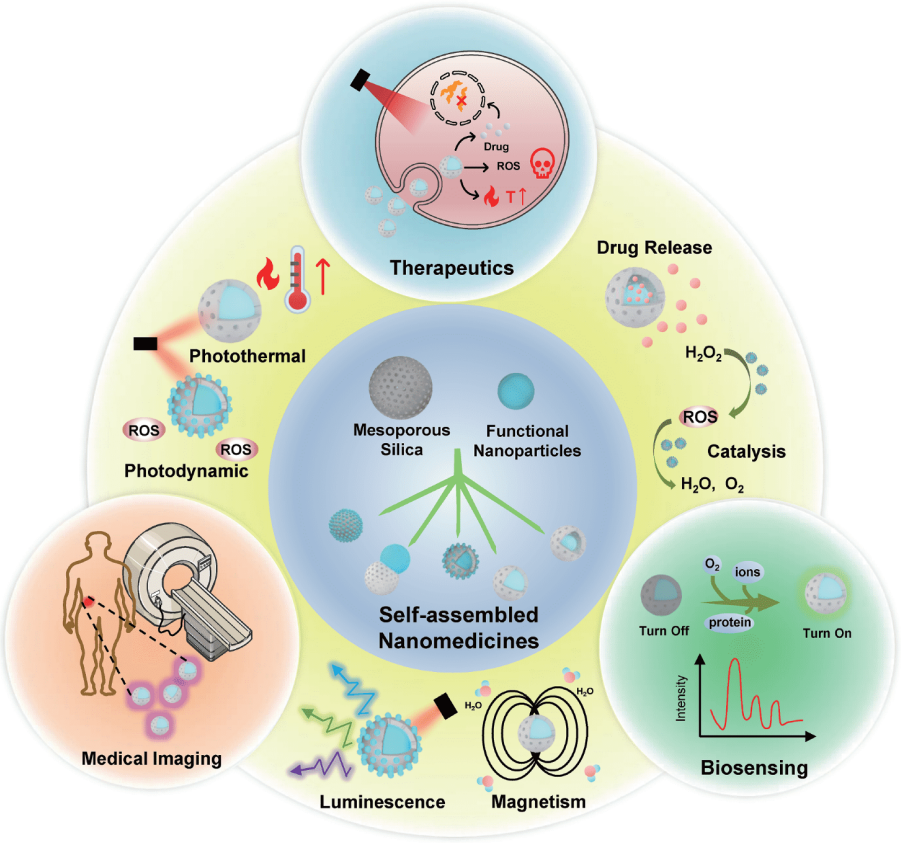


**Figure 1** Schematic illustration of the designs and biomedical applications of MSN-templated self-assembled theranostic nanomedicines. Self-assembled theranostic nanomedicines in heterostructure formation with multiple functions are fabricated by integrating different functional nanoparticles with MSN, which show great potential for diverse biomedical applications, such as biosensing, medical imaging and therapy (color online).

exhibit a good photothermal convention effect (Figure 2(d)). Moreover, MSN could also be embedded inside with functional component shell outside, which is usually used for stimuli-responsive drug release [43] and imaging [44].

### 2.2 Yolk-shell structure

Different from the core-shell structure, the functional core component of the MSN-based yolk-shell structure is located inside the hollow cavity of a silica shell. To create the void cavity, the template material is firstly coated on the surface of the core component prior to the formation of an MSN shell, then the template material could be selectively etched or removed to form the yolk-shell structure (Figure 3(a)) [45]. The synthetic method of yolk-shell nanoparticles can be roughly divided into the hard template method and the soft template method. For a soft template mediated process, various single/multi-surfactants are commonly used to cover the core component before MSN formation and can be easily removed during the extraction in an alcoholic solution containing salt to create the cavity. Although soft template method is a relatively simple strategy, it is not easy to precisely control the size of nanoparticles [13]. For hard template mediated process, the formation of the cavity is assisted by silylated compounds or metallic oxides such as ZnO which are subject to the etching in acidic pH or high temperature compared with MSN shell. For example, Huang *et al.* coated gold nanorod (GNR) core with a layer of ZnO followed by the formation of an outer MSN shell (Figure 3(b)). Uniform sized GNR was synthesized *via* a seed-mediated growing approach and used as a photoacoustic (PA) imaging and photothermal agent. ZnO layer served as a hard template that could be etched by HCl to form the yolk-shell GNR@$SiO_2$ nanorattle [46]. In some cases, the protecting agents are required for the controllable etching processes. Poly(vinylpyrrolidone) (PVP) is one of the surface protectors for MSN shell upon alkaline etching treatment. The hydroxyl ions can pass through the PVP protection layer and dissolve the inner silica shell to silicate oligomers, which are likely to immigrate and deposit in the PVP layer to form a new silica shell leaving a hollow cavity inside [47]. For example, Shi and co-workers firstly coated Gd doped UCNPs with a dense silica layer. Then, a mesoporous silica shell was deposited on the surface of Gd-UCNPs@d$SiO_2$ (Figure 3(c)). Based on the "surface-protected hot water etching" strategy, the outer mesoporous silica shell was protected by PVP, allowing the

**Table 1** Summary of the synthesis methods, structure properties, and applications of different MSN-templated self-assembled theranostic nanomedicines with various heterostructures.

| Heterostructures | Formulation | Synthetic methods | Structure properties | Applications | Ref. |
|---|---|---|---|---|---|
| Core-shell structure | UCNP@mSiO$_2$ | CTAC-assisted sol-gel reaction | High loading capacity with preserved luminescence | Light controlled drug release | [42] |
| | Fe$_3$O$_4$@MSN | CTAB-assisted sol-gel reaction | Enhanced biocompatibility with preserved magnetism | MRI contrast imaging | [36] |
| | Au@SiO$_2$ | CTAB-assisted sol-gel reaction | Enhanced biocompatibility with preserved photothermal effect | Photothermal therapy | [38] |
| | MSN@K$^+$-permeable membrane | Surface self-assembly | Selective ion permeation | Diagnosis and monitoring of epilepsy | [44] |
| | MnFe$_2$O$_4$@CoFe$_2$O$_4$@MSN | CTAB-assisted sol-gel reaction | High loading capacity with preserved magnetism | Alternating magnetic field controlled drug release | [82] |
| | RVGPEGAuNRs@SiO$_2$ | CTAB-assisted sol-gel reaction | Enhanced targeting ability with preserved photothermal effect | Photothermal therapey of brain tumor | [83] |
| | UCNP@MSN | CTAC-assisted sol-gel reaction | High loading capacity | Photodynamic immunotherapy | [88] |
| Yolk-shell structure | GNR@SiO$_2$ | Hard template etching | High loading capacity with preserved photothermal effect | PA imaging and photothermal therapy | [46] |
| | Gd-UCNPs@mSiO$_2$ | Surface-protected etching | High loading capacity with preserved magnetism and luminescence | Chemo-/radio-/photodynamic therapy and MR/UCL imaging | [48] |
| | UCNP@hmSiO$_2$ | Surface-protected etching | High loading capacity with preserved luminescence | Selective hypoxia detection | [68] |
| | UCNP@hmSiO$_2$ | Surface-protected etching | High loading capacity with preserved magnetism and luminescence | MRI and UCL monitored drug release | [74] |
| | Ln@SiO$_2$-ZnPc-DCs | Hard template calcination | High loading capacity with preserved magnetism and optical properties | MR/UCL/CT/PT imaging and chemo-/photothermal/photodynamic therapy | [77] |
| Core-satellite structure | DOX@MSN-WS$_2$-HP | Noncovalent conjugation | High loading capacity with preserved photothermal effect | pH-responsive drug release and photothermal therapy | [52] |
| | MSN-manganese ferrite/ ceria NPs | Covalent conjugation | Enhanced $O_2$ generation and ROS scavenging | Treatment of rheumatoid arthritis | [56] |
| | MSN-Ceria | Covalent conjugation | Enhanced biocompatibility and ROS scavenging | Wound healing | [57] |
| | MSN-QDs/CDs | Covalent conjugation | Enhanced biocompatibility and sensitivity | Intracellular $Cu^{2+}$ sensing | [70] |
| | CeNC/IONC/MSN-T807-MB | Covalent conjugation | High loading capacity with preserved magnetism and ROS scavenging effect | Treatment of Alzheimer's disease | [51] |
| | $^{89}$Zr-HMSN-CuS | Noncovalent conjugation | High loading capacity with preserved photothermal effect | PET imaging and photothermal/photodynamic therapy | [76] |
| | DSF@PEG/Cu-HMSNs | *In-situ* doping | High loading capacity with preserved catalytic activity | Chemotherapy and chemodynamic therapy | [84] |
| Heterodimer structure | GNR-mSiO$_2$ | CTAB-assisted anisotropic growth | High loading capacity with preserved optical properties | Chemoradiotherapy and CT imaging | [61] |
| | Fe$_3$O$_4$-MON | CTAB-assisted anisotropic growth | High loading capacity with preserved magnetism | Photodynamic therapy, magnetic hyperthermia and immunotherapy | [62] |
| | Fe$_3$O$_4$-MSN | CTAB-assisted anisotropic growth | High loading capacity with preserved magnetism | MRI and hyperthermia-enhanced gene therapy | [78] |
| Core-Shell-Satellite structure | AuNR@MS@AgNPs | CTAB-assisted sol-gel reaction and *in-situ* growth | High loading capacity with preserved photothermal effect | GSH-responsive drug release and photothermal/ photodynamic therapy | [64] |
| | Au@MSN@IONP | CTAB-assisted sol-gel reaction and covalent conjugation | Enhanced biocompatibility with preserved magnetism, catalytic activity and photothermal effect | Photothermal/chemodynamic therapy | [85] |

inner layer of dense silica to be etched out [48]. Owing to the unique structural feature, the as-synthesized yolk-shell nanoparticles obtain an additional cargo loading capacity, promising for theranostics [49].

### 2.3 Core-satellite structure

Fabrication of nanoparticles with a core-satellite structure is an alternative way to assemble multiple components onto a

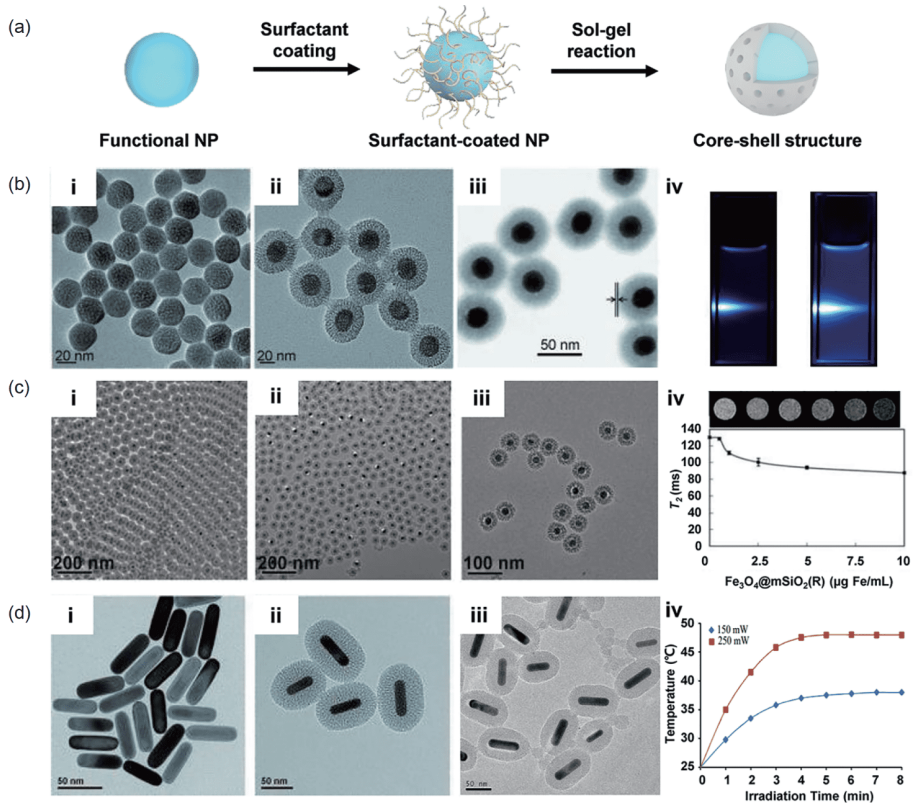


**Figure 2** MSN-templated theranostic nanomedicines with core-shell structures. (a) Schematic illustration of the synthetic strategy of core-shell structured nanomedicines. (b) TEM images of i) $NaYF_4$:Tm,Yb@$NaYF_4$; ii) UCNP@$mSiO_2$; iii) bright-field STEM image of TAT-modified UCNP@$mSiO_2$-azo; iv) digital photos of $NaYF_4$:Tm,Yb@$mSiO_2$ and $NaYF_4$:Tm,Yb@$NaYF_4$@$mSiO_2$ under NIR laser excitation. Reproduced with permission from ref. [42]. (c) TEM images of i) 53 nm $Fe_3O_4$@$mSiO_2$ with 15 nm core; ii, iii) 45 nm $Fe_3O_4$@$mSiO_2$ with 22 nm core; iv) $T_2$-weighted MR images of $1.2\times10^6$ MCF-7 cells labelled with $Fe_3O_4$@$mSiO_2$(R)-PEG at various concentrations for 1 h. Reproduced with permission from ref. [36]. (d) TEM images of i) AuNRs; ii, iii) Au@$SiO_2$; iv) The photothermal effect of Au@$SiO_2$. Reproduced with permission from ref. [38] (color online).

single silica template. The method to fabricate core-satellite nanoparticles is the utilization of conjugation ligands for the attachment of functional components on the silica template, which permits the well synthesized functional components to be flexibly decorated [30]. Besides, functional nanoparticles can be *in-situ* grown onto the surface of MSN during the synthetic process as long as the interface energy is favorable (Figure 4(a)) [30]. The nanocomposites in the core-satellite morphology are capable of endowing the system with more properties. Surface-decorated nanoparticles can serve independently as imaging agents [50], catalysts [51], photothermal agents[52, 53], *etc.* or work together for synergistic effects. Meanwhile, they can be designed to function as gatekeepers that are responsive to internal/external stimuli. This avoids the early leakage of drugs by having stringent control over drug release from the nanocomposites [54,55]. Lei and co-workers [52] designed a size-controllable "cluster bomb" (DOX@MSN-$WS_2$-HP). MSN were firstly synthesized by the sol-gel reaction and then functionalized with 4-adamantane carboxylate benzaldehyde to prepare acid-labile MSN-Benzoic-Imine-Ad (MSN-Ad). Tungsten disulfide ($WS_2$) quantum dots were synthesized and modified with β-CD through the W–S bond and further conjugated with a short peptide tLyP-1 ($WS_2$-HP). Drug-loaded DOX@MSN-$WS_2$-HP was finally assembled *via* host-guest interaction between adamantane and β-CD. $WS_2$-HP can act as gatekeepers of DOX and photothermal agents (Figure 4(b)). Hyeon group [56] co-decorated manganese ferrite and ceria nanoparticles onto MSN forming core-satellite structure nanomedicines. The satellite manganese ferrite and ceria nanoparticles served as catalysts for effective ROS scavenging and $O_2$ generation. Besides, our group also designed ceria nanoparticles decorated MSN (MSN-Ceria), which exhibited excellent property in catalyzing ROS to $H_2O$ for wound healing (Figure 4(c)) [57].

### 2.4 Heterodimer structure

Heterodimer nanoparticles, namely Janus nanoparticles, integrate two different functional components into one single system with an asymmetric morphology [58,59]. Heterodimer structure is energetically favored during anisotropic growth when the interface energy between two components is relatively high (Figure 5(a)) [60]. Nowadays, the MSN

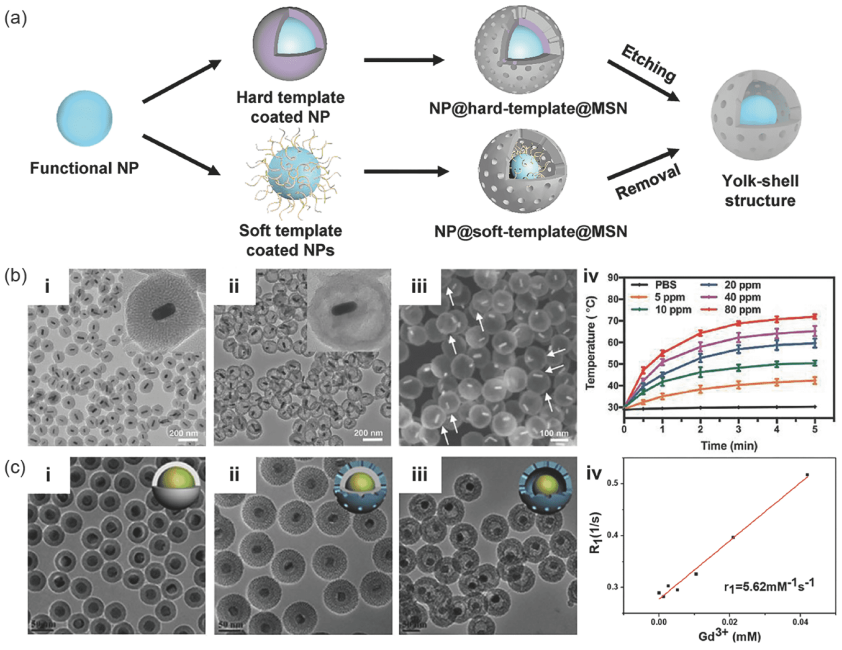


**Figure 3** MSN-templated theranostic nanomedicines with yolk-shell structure. (a) Schematic illustration of the synthetic strategy of yolk-shell structured nanomedicines. (b) TEM images of i) GNR@ZnO; ii) GNR@$SiO_2$; iii) SEM image of GNR@$SiO_2$; iv) temperature elevation curves of PBS and GNR@$SiO_2$ solution of different concentrations under 808 nm laser irradiation. Reproduced with permission from ref. [46]. (c) TEM images of i) Gd-UCNPs@d$SiO_2$; ii) Gd-UCNPs@d$SiO_2$@m$SiO_2$ and iii) UCMSNs; iv) plots of $R_1$*versus* $Gd^{3+}$ concentrations for UCMSNs in aqueous solution. Reproduced with permission from ref. [48] (color online).

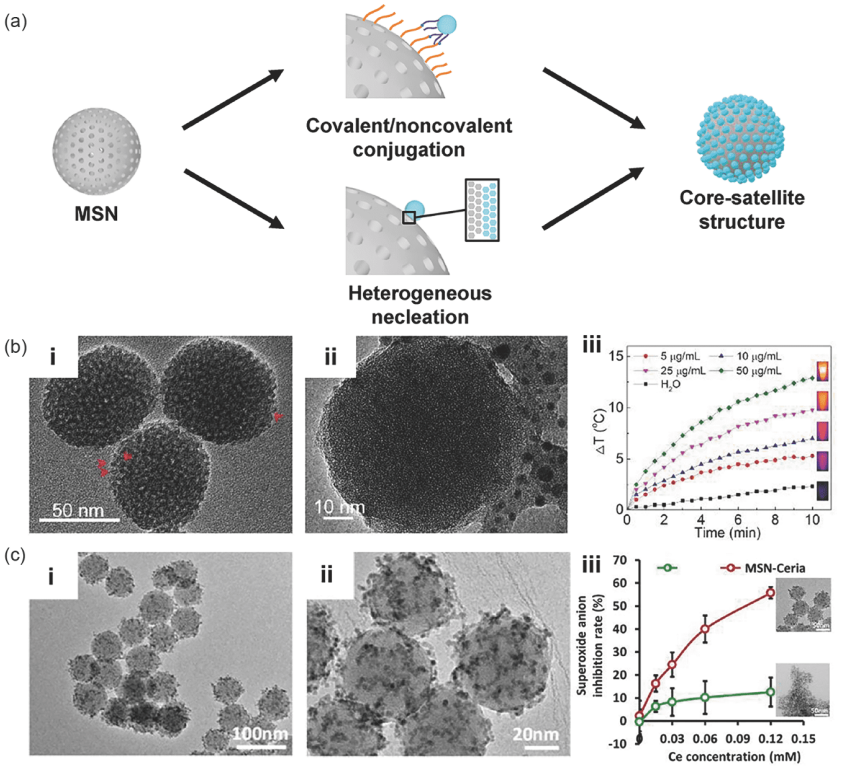


**Figure 4** MSN-templated theranostic nanomedicines with core-satellite structure. (a) Schematic illustration of the synthetic strategy of core-satellite structured nanomedicines. (b) TEM images of i) DOX@MSN-$WS_2$-HP and ii) DOX@MSN-$WS_2$-HP pretreated at pH 6.8; iii) temperature changes of $WS_2$-HP at different concentration with NIR irradiation. Reproduced with permission from ref. [52]. (c) i) TEM and ii) HRTEM images of MSN-Ceria nanocomposite; iii) neutralization of superoxide anions by MSN-Ceria in a dose-dependent manner compared with ceria aqueous suspension. Reproduced with permission from ref. [57] (color online).

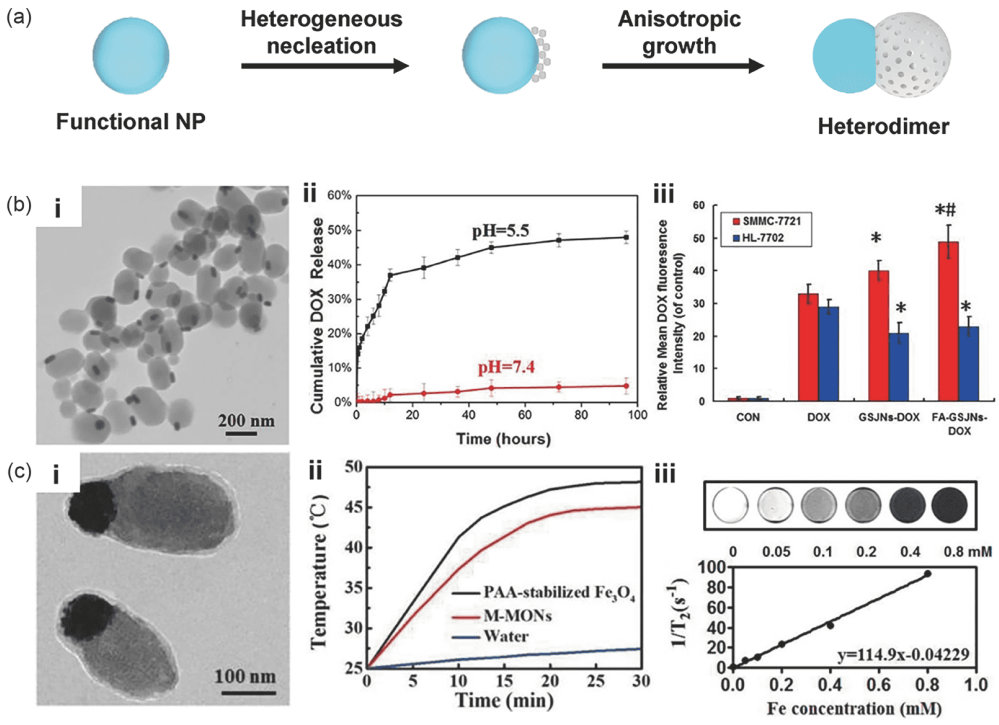


**Figure 5** MSN-templated theranostic nanomedicines with heterodimer structure. (a) Schematic illustration of the synthetic strategy of heterodimer structured nanomedicines. (b) i) TEM image of FA-GSJNs; ii) pH-dependent drug-release profiles of FA-GSJNs-DOX; iii) quantitative analysis of the fluorescence intensity of DOX in free DOX-, GSJNs-DOX-, or FA-GSJNs-DOX-treated SMMC-7721 or HL-7702 cells for 3 h. Reproduced with permission from ref. [61]. (c) i) TEM image of CM@M-MON@Ce6; ii) temperature-time curves of M-MONs; iii) MR images of CM@M-MON@Ce6 with different concentrations of Fe and plots of the inverse transverse relaxation time ($1/T_2$) *versus* the Fe concentration of the CM@M-MON@Ce6. Reproduced with permission from ref. [62] (color online).

based anisotropic Janus nanoparticles with multiple components are rationally designed and investigated for disease theranostics. The MSN component can accommodate large amounts of therapeutic agents, while the other component can serve as imaging agents. For example, Dong and co-workers [61] developed a heterodimer gold nanorod-mesoporous silica nanoparticle (GSJN) with gold nanorod head and $mSiO_2$ body. Gold nanorod (GNR) was first prepared *via* the seed growth method, and the Janus-structure-like GSJN was further obtained by the CTAB-templated sol-gel approach. After DOX loading and folic acid modification, the resulting FA-GSJNs-DOX displayed excellent hepatocellular carcinoma cells (HCC) targeting ability and a pH-responsive drug release (Figure 5(b)). Wang and co-workers reported bullet-like Janus magnetic mesoporous organosilica nanoparticles (M-MONs) for MRI-guided anti-metastatic immunotherapy (Figure 5(c)). $Fe_3O_4$ nanospheres were firstly synthesized, and through a CTAB-templated sol-gel approach, disulfide-bridged mesoporous organosilica rods were asymmetrically grown on the surface of $Fe_3O_4$ nanosphere [62]. The resulting Janus nanoparticles with asymmetric chemistry and structures, can achieve stimuli responsive drug release and MRI guided photodynamic therapy (PDT)/magnetic hyperthermia for cancer theranostics.

## 2.5 Core-shell-satellite structure

To endow the nanomedicines with multifunctionality, core-shell and core-satellite structures could be combined to develop versatile theranostic agents, namely core-shell-satellite nanoparticles [63]. The satellite components could be assembled onto the surface of MSN after the formation of a core-shell structure (Figure 6(a)). The combination of functional components integrates the different properties such as catalysis, imaging and photothermal effect for improved theranostic performance. Zhang and co-workers [64] synthesized the multifunctional core-shell-satellite nanoparticles (AuNR@MS@AgNPs) by the in-situ growth of silver nanoparticles on the surface of MSN-coated gold nanorods (Figure 6(b)). The AgNPs on the surface act as glutathione (GSH) responsive capping agents under GSH enriched tumor environment for the controlled release of PDT agents. Upon NIR irradiation, this core-shell-satellite nanoplatform exhibited combined photothermal/photodynamic therapy with improved anti-cancer efficiency.

Taken together, the various heterostructures of MSN-templated self-assembled nanomaterials can be prepared by

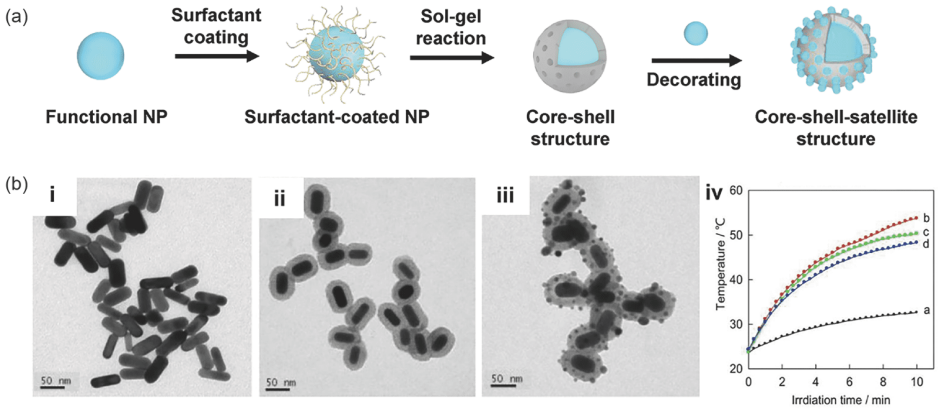


**Figure 6** MSN-templated theranostic nanomedicines with core-shell-satellite structure. (a) Schematic illustration of the synthetic strategy of core-shell-satellite structured nanomedicines. (b) TEM images of i) AuNRs; ii) AuNR@MS and iii) AuNR@MS@AgNP; iv) temperature-time curves of PBS buffer (black), PBS buffer+AuNR (red), PBS buffer+AuNR@MS (green) and PBS buffer+AuNR@MS@AgNP (blue). Reproduced with permission from ref. [64] (color online).

different combination methods. The resulting nanosystems with diverse properties in optics, magnetics, catalysis, drug loading, *etc*. are competent for various biomedical applications.

## 3 Applications of MSN-templated self-assembled theranosticnanomedicines

Recently, various MSN-templated self-assembled nanomedicines have been developed and applied for biomedical applications due to their unique structural properties. The MSN usually play the role of drug carriers that can protect the cargos from rapid elimination and thus improve their accumulation in the targeted sites [35,65]. Coupled with protection, the functional nanocomponent can serve as imaging or therapeutic agents for disease theranostics [30]. The co-assembly of MSN and functional nanoparticles endows the nanosystem with improved biocompatibility and multifunctionality, meeting the growing demands for intelligent theranostics. In this section, we discuss the strategies to use MSN-templated nanomedicines for biosensing, medical imaging and therapeutics.

### 3.1 Biosensing

MSN-based nanomedicines are widely investigated in sensing owning to their optical properties and hierarchical structures [66]. MSN could be an ideal carrier for the loading of optical sensors/indicators on the surface or inside mesoporous pores. The integration of functional nanocomponents improves sensitivity and selectivity [67]. Besides, the morphological characteristics of the nanosensors determine their functionalities and applications. For example, biosensing molecules can be encapsulated in the hollow cavity of yolk-shell structured nanosensor and can intact with the external environment through the pores of the MSN shell. Shi and co-workers developed a yolk-shell structured nanosensor by encapsulating UCNP core and oxygen indicators tris (4,7-diphenyl-1,10-phenanthroline) ruthenium (II) dichloride (designated as $[Ru(dpp)_3]^{2+}Cl_2$) in the hollow MSN for the detection of oxygen in hypoxic regions. Under NIR irradiation, the emission from UCNPs can activate $[Ru(dpp)_3]^{2+}Cl_2$, exhibiting reversibly quenched or illuminated manners under hyperoxic or hypoxic conditions. Notably, in contrast to free oxygen indicators, the as-prepared nanosensors showed enhanced sensitivity for the detection of oxygen in hypoxic regions without the disturbances from acidic and reducing tumor intracellular microenvironment [68].

In addition, core-shell nanostructures have also been used for biosensing as the shell components can enhance the sensing selectivity by the selective entrance of ions from the outside environment. Our group coated MSN with a unique ultrathin layer of $K^+$-permeable membrane filter for highly sensitive and specific $K^+$ sensing [44]. The $K^+$-permeable membrane filter formed by controlled self-assembly of three-dimensional tripodal ligands can selectively capture $K^+$, thus the $K^+$ indicators loaded inside MSN can exclusively measure the dynamics of $K^+$ level without the interference from other cations. Moreover, this $K^+$-sensitive nanosensor can convey the spatiotemporal information about extracellular $K^+$ concentration in multiple brain regions of freely moving mice, enabling the monitoring of neural activity in the brain (Figure 7). The $K^+$ sensitive nanosensors have shown great potential in the early diagnosis of epilepsy and accurate monitoring of epileptic seizures, which can guide the rational use of anti-epileptic drugs for achieving precise treatment of epilepsy with reduced side effects.

Moreover, nanosensors decorated onto MSN can promote the access of surrounding substances for the specific sensing of biochemicals [69]. Han and co-workers synthesized core-satellite structured nanoprobes by decorating two fluorescent

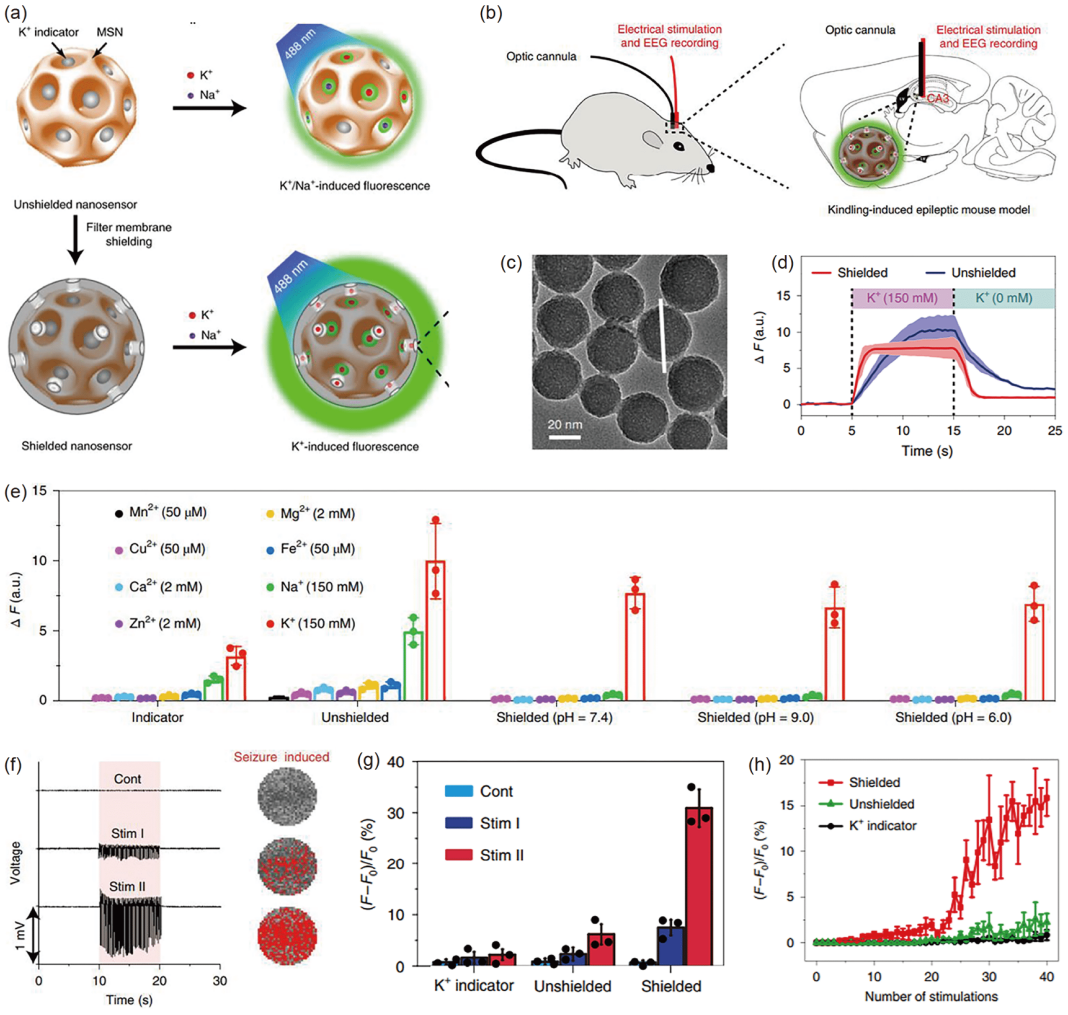


**Figure 7** MSN-templated theranostic nanomedicines for biosensing. (a) Schematic illustration of the $K^+$ nanosensor. (b) *In vivo* experimental scheme for $[K^+]_o$ sensing in a kindling-induced epileptic mouse model. (c) TEM images of shielded nanosensors. (d) Time-dependent changes in the nanosensor fluorescence intensity on the incubation in $K^+$-rich and $K^+$-free aqueous solutions. (e) Fluorescence changes in the presence of different ions. (f) Extracellular fluorescence responses (right) for the given electrical pulses of different intensities (left). The red dots represent the extracellular regions where the signal responses ($\Delta F/F_0$) are greater than 5%. (g) Quantification of fold changes in peak fluorescence response in (f). (h) Relationship between the changes in amplitude of the nanosensor fluorescence signal and the number of stimulations. Reproduced with permission from ref. [44] (color online).

nanodots (quantum dots (QDs) and carbon dots (CDs)) on the surface of MSN for intracellular $Cu^{2+}$ imaging. The red-emitting QDs were attached to the MSN to serve as the response signal label, while the blue-emitting CDs were attached to the QDs as the reference signal label. The MSN carriers not only improved the stability and brightness of QDs significantly but also tremendously decreased the cytotoxicity toward HeLa cells. The red emission from QDs could be quenched by $Cu^{2+}$ without influencing the blue emission from CDs. Consequently, according to the linear decrease of the red/blue signal ratio, the intracellular $Cu^{2+}$ could be detected with improved sensitivity [70].

### 3.2 Medical imaging

Recently, MSN-based nanomedicines have shown promising applications in various diagnostic modalities such as MRI, upconversion luminescent (UCL) imaging, ultrasonic (US) imaging, computerized tomography (CT) imaging, positron emission tomography (PET) imaging, for early diagnose of diseases, providing optimal therapeutic guidances as well as post-treatment monitorings for enhanced therapeutic efficacy [71]. MRI is a typical imaging technique that has been widely used in clinical settings to offer images with high spatial resolution and superior soft tissue contrast [72]. MR contrast agents can be encapsulated inside the MSN or controlled assembly on the surface of MSN with good dispersibility and enhanced contrasting effect [27]. Our group reported a core-satellite nanocomposite (CeNC/IONC/MSN-T807-MB) for the treatment of Alzheimer's disease (AD). Ultrasmall ceria nanocrystals (CeNCs) and iron oxide nanocrystals (IONCs) were co-assembled on the surface of

MSN. The tau tracer amino-T807 was grafted onto the surface of MSN *via* the conjugation of $^{68}$Ga-labeled macrocyclic chelator 1,4,7-triazacyclononane-1,4,7-triacetic acid, resulting in the specific binding of nanocomposite to hyperphosphorylated tau. IONCs on the surface of MSN were used as high-performance MRI contrast agents for tauopathy. Moreover, CeNCs companied with methylene blue (MB), significantly inhibited tau hyperphosphorylation and aggregation. Such core-satellite-structured theranostic nanocomposites possess great potential in MRI/PET bimodal imaging guided AD combinational therapy (Figure 8(a)) [51].

Optical imagings with high sensitivity were also extensively used for diagnostics. However, the current fluorescent probes are hindered by the low penetration depth of the exciting light. Recently developed lanthanide-doped UCNP, which converts NIR light to visible light, is a feasible tool for deep tissue imaging [73]. The coating of MSN preserves the optical performance of UCNPs and improves its biocompatibility. For example, Shi and co-workers prepared DOX-loaded yolk-shell structured UCNP@hm$SiO_2$ through the hard-template method for real-time monitoring of drug release. They utilized the designed luminescence resonance energy transfer (LRET) donor-acceptor pair of the UCNP and DOX for monitoring drug release in real-time by detecting UCL signals. Moreover, the release of DOX residing in the hollow cavity allowed the $T_1$-weighted MR signal enhancement for quantifying the drug release. Such yolk-shell nanocomposites realized the visualization of quantification of drug release *in vitro* and *in vivo* by real-time MR/UCL dual-mode imaging [74].

PET imaging is an emerging diagnostic modality with ultra-high sensitivity that can be used for molecular imaging [75]. MSN-based radiolabeled nanomaterials have been widely explored in PET imaging. Cai and co-workers reported a multifunctional core-satellite nanocomposite by assembling CuS nanoparticles on the surface of porphyrin loaded $^{89}$Zr-labeled hollow mesoporous silica nanoparticles (HMSN). HMSN as the template could enhance the solubility and bioavailability of meso-tetrakis(4-carboxyphenyl) porphyrin and improve the blood residence and tumor accumulation of ultrasmall CuS. The labeling of $^{89}$Zr endowed the system with PET guided cancer therapy (Figure 8(b)) [76]. In particular situations, it is necessary to combine multiple imaging probes for more comprehensive diagnostic requirements. For instance, Lin and co-workers incorporated

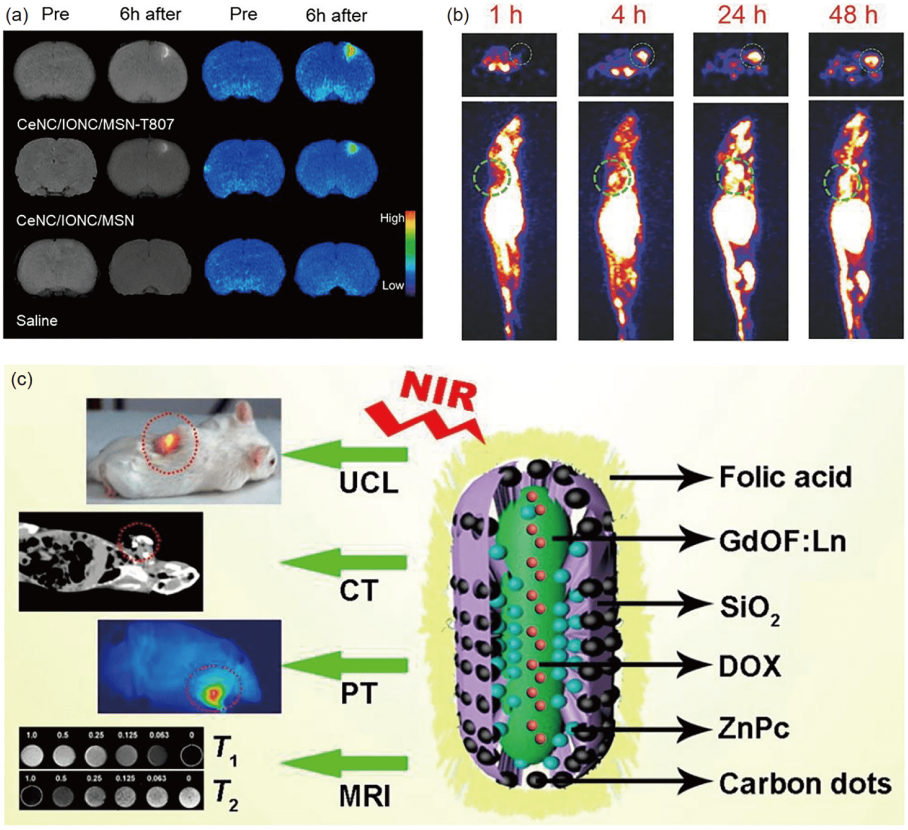


**Figure 8** MSN-templated theranostic nanomedicines for medical imaging. (a) *In vivo* MR images of the brain of AD rats after 6 h post-injection (left) and the corresponding colors mapped images (right). Reproduced with permission from ref. [51]. (b) *In vivo* PET imaging with [$^{89}$Zr]CSNC-$PEG_{10k}$. Reproduced with permission from ref. [76]. (c) Schematic illustration for the bio-application of GdOF:Ln@$SiO_2$-ZnPc-CDs microcapsule and for multiple imaging. Reproduced with ref. [77] (color online).

UCNPs into carbon dots attached MSN shells to obtain yolk-shell structured nanocomposites (GdOF:Ln@$SiO_2$-ZnPc-DCs). The doped rare-earth ions in the core endow the nanocomposite with excellent UCL, MRI and CT imaging properties. Besides, carbon dots with an excellent photothermal effect under NIR laser irradiation can serve as photothermal (PT) imaging agents (Figure 8(c)). This unique nanosystem with multimodal imaging and therapeutic properties is promising for cancer theranostics [77].

### 3.3 Therapeutics

MSN-based nanomedicines have attracted enormous attention as they have demonstrated ascendant advantages in disease therapy [13]. The delivery of therapeutic agents such as chemotherapeutic drugs or nucleic acids using MSN enables enhanced targeting efficiency. Dong and co-workers fabricated and compared two differently shaped magnetic mesoporous silica nanoparticles (M-MSN) for the combined suicide gene/magnetic hyperthermia therapy of HCC. The rod-like Janus M-MSN showed relatively higher gene-loading efficiency, faster gene-release behavior and enhanced gene delivery under external magnetic fields, resulting in superior magnetic targeting and magnetic hyperthermia-enhanced suicide gene therapeutic performance against HCC [78]. Moreover, the integration of stimuli responsive components endows MSN-based nanomedicines with noninvasive stimuli triggered drug delivery manner [79–81]. Chen *et al.* reported an alternating magnetic field (AMF) responsive drug release system by encapsulating a superparamagnetic Mn/Co doped iron oxide ($MnFe_2O_4$@$CoFe_2O_4$) core into an MSN shell. The MSN shell modified with thermo-responsive molecule-based gatekeepers was used for DOX accommodation. After the exposure to AMF, the $MnFe_2O_4$@$CoFe_2O_4$ core generated efficient magnetic heating for the cleavage of gatekeepers, realizing AMF-triggered drug release. Moreover, the dosage of released DOX can be externally controlled by tuning the exposure time of AMF, showing great potential for the stimuli-triggered spatial and temporal control of drug release [82].

Besides, other organic/inorganic functional materials with excellent photothermal capacity or the catalytic activity for the generation of intratumoral ROS can be integrated for augmented therapeutic effects. Lee and co-workers reported a core-shell nanoparticle by embedding gold nanorod (AuNR) in an MSN shell (RVGPEGAuNRs@$SiO_2$) for glioma treatment. The synthesized AuNRs@$SiO_2$ were surface modified with rabies virus glycoprotein 29 (RVG29) for passing the blood-brain-barrier (BBB) and entering the brain through the nicotinic acetylcholine receptor (AchR). The AuNR cores can increase their interaction with the nicotinic AchR and generate heat under NIR light irradiation. The as-synthesized rabies virus mimic nanoparticle exhibited excellent photothermal effect for brain tumor targeted therapy [83]. Wu and co-workers demonstrated a tumor specific "nontoxicity-to-toxicity" transition strategy based on $Cu^{2+}$-doped, disulfiram (DSF)-loaded hollow MSN for cancer therapy. Once the DSF-loaded hollow MSN were endocytosed into tumor cells, $Cu^{2+}$ ions and DSF were rapidly released due to the biodegradation of the nanoparticles in the acidic tumor microenvironment. The toxic CuET products were generated by *in situ* chelation between $Cu^{2+}$ and DSF, and ROS were then generated by $Cu^{+}$-mediated Fenton-like reaction, showing great potential for Cu-enhanced chemodynamic therapy of cancer [84].

Moreover, integrated theranostic nanomedicines with combined functions are excepted to achieve synergistically enhanced therapeutic efficiency. For example, our group reported core-shell-satellite nanomaces (Au@MSN@IONP) fabricated by the self-assembly of ultrasmall iron oxide nanoparticles (IONP) on the surface of MSN-coated gold nanorod (Au@MSN) [85]. The Au nanorods were synthesized through the seeding growth method, and the uniform mesoporous silica shell was deposited on the Au nanorods *via* the Stöber process. The monodispersed ultrasmall bromine-modified IONPs were assembled onto the amino-modified mesoporous silica shell through nucleophilic substitution reaction. The embedded Au nanorods served as photothermal conversion agents that can generate heat under laser irradiation to elevate the intracellular $H_2O_2$ level. Meanwhile, IONPs at the outer layer can catalyze the elevated $H_2O_2$ to cytotoxic hydroxyl radicals for cancer cell killing. Moreover, IONPs could also be used as MRI contrast agents to monitor the tumor accumulation of the nanomaces, and thus optimize the time point of light irradiation. By utilizing the vulnerability of iron efflux in triple-negative breast cancer (TNBC) cells, Au@MSN@IONP nanomaces exhibited a synergistic anti-TNBC efficacy with minimized side effects (Figure 9).

Recently, immunotherapy is considered as one of the most promising therapeutic approaches that has revolutionized the treatment of previously incurable diseases [86]. Immunomodulatory agents such as antigens and adjuvants are developed to activate the cascade of immune response for disease treatments, and various nanocarriers are fabricated for the targeted delivery of these immunomodulatory agents to specific tissues and cells [87]. MSN-based nanomedicines with self-adjuvanticity and structural properties could be designed as nanovaccines for the delivery of immunomodulatory agents. Lin and co-workers prepared large-pore MSN coated UCNPs (UCMSs) as novel immunoadjuvants for cancer therapy. MSN could encapsulate photosensitizer merocyanine 540 (MC540), model proteins (chicken ovalbumin (OVA)) and tumor antigens (tumor cell fragment (TF)) with high loading capacities. Upon NIR irradiation, UCMSs-MC540-OVA showed the synergistic

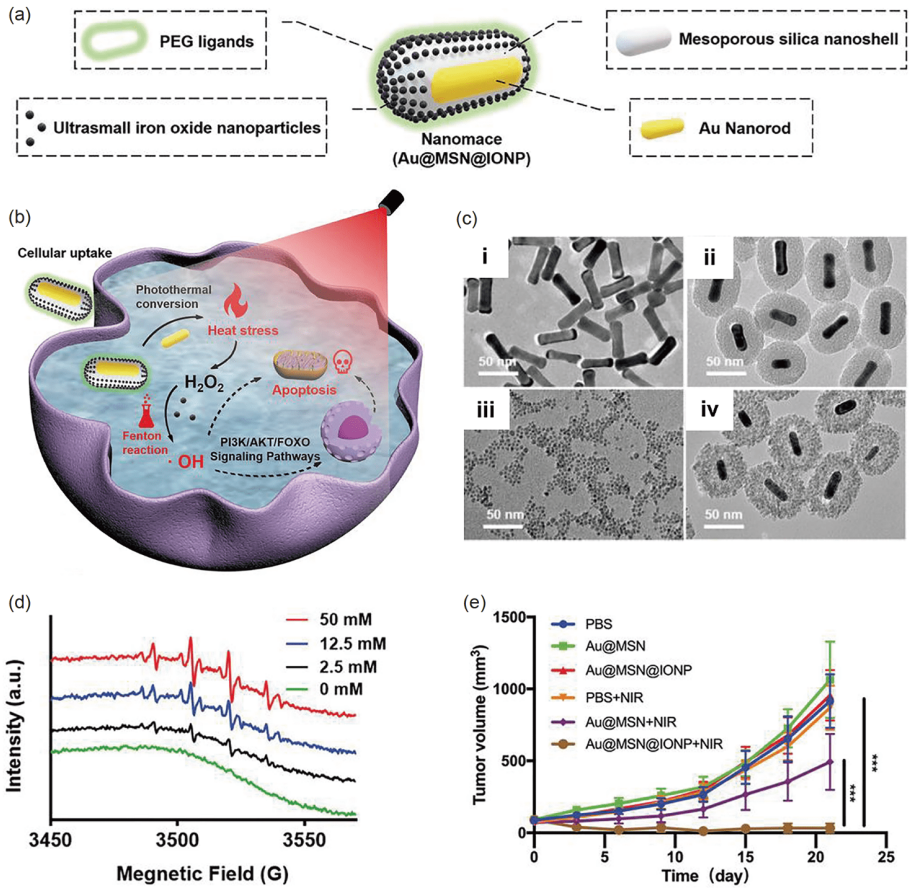


**Figure 9** MSN-templated theranostic nanomedicines for therapeutics. (a) Schematic illustration of Au@MSN@IONP and (b) therapeutic mechanism for TNBC. (c) TEM images of i) Au nanorods, ii) Au@MSN, iii) IONPs and iv) Au@MSN@IONP. (d) ESR spectra of Au@MSN@IONP with the addition of various concentrations of $H_2O_2$. (e) Tumor growth curves of mice after various treatments. Reproduced with permission from ref. [85] (color online).

immunopotentiation action to activate Th1 and Th2 immune responses and regulate immunity-associated cells. Moreover, UCMSs-MC540-TF effectively inhibited the tumor growth and prolonged the lifetimes of CT26-tumor-bearing BALB/c mice by the combination of PDT and immunological therapy, indicating the great potential of UCMSs as immunoadjuvants for clinical cancer treatment [88].

## 4 Conclusions and perspective

The fabrication strategies of MSN-based theranostic nanomedicines for diagnosis, monitoring and treatment of diseases are continuously advancing. As excellent templates, MSN are capable of assembling different functional components and concurrently revealing their potentials in the accomplishment of the tasks that are clinically in demand. Most existing review papers related to MSN are focused on their specific functions as well as their applications in drug delivery and targeted therapy. Here, we overview the strategy for the fabrication of MSN-templated theranostic nanomedicines with a focus on the designed assembly of diverse functional nanoparticles. Based on the rationally designed combination methods and structure regulations, the functional nanomaterials could be integrated into one single system with enhanced biocompatibility and performance in disease theranostics.

Nevertheless, there remain several challenges to overcome before practical clinical applications of MSN-templated self-assembled nanomedicines. Firstly, the effects of physical and chemical parameters, including the size, shape, surface chemistry of self-assembled nanomedicines, on their cellular uptake, transportation and bioviability are not well understood yet. Therefore, the establishment of structure/property relationships between MSN-templated self-assembled nanomedicines and their biological functions is essential to customize the nanomedicines for personalized theranostics. For instance, nanomaterials with enzymatic activities have been used to regulate the signaling molecules such as ROS. These nanomaterials can be attached on the surface of MSN, be confined in the pores of MSN, or be coated with MSN shell. The comparative studies of different combination strategies and the resulting structures on intracellular ROS regulation are highly valuable for the better design of cut-

ting-edge enzymatic MSN-templated self-assembled nanomedicines. Besides, the difference of morphological structures of MSN-based nanomedicines on immunological stress in biosystems is important yet rarely investigated. Further in-depth studies in this filed are beneficial to the development of MSN-based antigens and vaccines for personalized immunotherapy. Moreover, the utilization of chemoinformatics and bioinformatics to study the biological interactions of MSN-templated self-assembled nanomedicines *via* computer simulations may contribute to the screening of the optimistic formulation of self-assembled nanomedicines for specific biomedical applications. Secondly, the integration of multiple therapeutic or diagnostic modalities in MSN-templated self-assembled nanomedicines inevitably sets high demands on the merging of different types of equipments that offer the multi-imaging modality to effectively wield these multifunctional weapons. Finally, the degradation and long-term biosafety of MSN have been well investigated. However, the biosafety evaluation of the functional nanocomponents integrated in MSN-templated self-assembled nanomedicines is often fragmented. The influences of integrated nanocomponents on *in vivo* biological absorption, distribution, metabolism and excretion must be fully investigated before clinical translations. Besides, there is a huge difference between currently used animal disease models and clinical patients. As a result, the assays on animal models with better reference parameters [89], such as macaque should be taken into consideraton. In addition, the evaluation indexes of the biosafety assays should involve more chronic and specific toxicity, such as reproductive toxicity and neurotoxicity to identify the potential risks [90]. Only when we comprehensively understand the biosafety of MSN-templated self-assembled nanomedicines, do we begin to translate these smart nanomedicines in clinical applications.

In conclusion, the assembly strategies and various heterostructures as presented in this review allow us to better understand the assembly mechanisms and structural functions of MSN-templated self-assembled nanomaterials, which is beneficial for the further design of intelligent nanomedicines with advanced theranostic performance. The multidisciplinary efforts from researchers of different research fields including material science, chemistry, pharmaceutics, toxicology, nano-biological interactions, immunology, bioengineering and medicine are expected to bring these prevailing paradigms towards clinical translation of MSN-templated self-assembled nanomedicines in near future.

**Acknowledgements** This work was support by the National Key Research and Development Program of China (2016YFA0203600), the National Natural Science Foundation of China (31822019, 32071374, 51703195, 91859116), the One Belt and One Road International Cooperation Project from Key Research and Development Program of Zhejiang Province (2019C04024), the Zhejiang Provincial Natural Science Foundation of China (LGF19C100002), the National Science & Technology Major Project 'Key New Drug Creation and Manufacturing Program', China (2018ZX09711002), and the Fundamental Research Funds for the Central Universities (2019XZZX004-15, 2020FZZX001-05).

**Conflict of interest** Conflict of interest The authors declare no conflict of interest.

1 Soares S, Sousa J, Pais A, Vitorino C. *Front Chem*, 2018, 6: 360
2 Kim BYS, Rutka JT, Chan WCW. *N Engl J Med*, 2010, 363: 2434–2443
3 Lin G, Mi P, Chu C, Zhang J, Liu G. *Adv Sci*, 2016, 3: 1600134
4 Barenholz YC. *J Control Release*, 2012, 160: 117–134
5 Lee N, Yoo D, Ling D, Cho MH, Hyeon T, Cheon J. *Chem Rev*, 2015, 115: 10637–10689
6 Wong XY, Sena-Torralba A, Álvarez-Diduk R, Muthoosamy K, Merkoçi A. *ACS Nano*, 2020, 14: 2585–2627
7 Lim EK, Kim T, Paik S, Haam S, Huh YM, Lee K. *Chem Rev*, 2015, 115: 327–394
8 Choi KY, Liu G, Lee S, Chen X. *Nanoscale*, 2012, 4: 330–342
9 Kim H, Kwak G, Kim K, Yoon HY, Kwon IC. *Biomaterials*, 2019, 213: 119207
10 Xie J, Lee S, Chen X. *Adv Drug Deliver Rev*, 2010, 62: 1064–1079
11 Vallet-Regi M, Rámila A, del Real RP, Pérez-Pariente J. *Chem Mater*, 2001, 13: 308–311
12 Yang B, Chen Y, Shi J. *Mater Sci Eng-R-Rep*, 2019, 137: 66–105
13 Tang F, Li L, Chen D. *Adv Mater*, 2012, 24: 1504–1534
14 Liang J, Liang Z, Zou R, Zhao Y. *Adv Mater*, 2017, 29: 1701139
15 Zheng H, Gao F, Valtchev V. *J Mater Chem A*, 2016, 4: 16756–16770
16 Parra-Nieto J, del Cid MAG, Cárcer IA, Baeza A. *Biotechnol J*, 2020, 2000150
17 Chen W, Glackin CA, Horwitz MA, Zink JI. *Acc Chem Res*, 2019, 52: 1531–1542
18 Garcia-Bennett AE. *Nanomedicine*, 2011, 6: 867–877
19 Manzano M, Vallet-Regí M. *Adv Funct Mater*, 2020, 30: 1902634
20 Kankala RK, Han Y-, Na J, Lee C-, Sun Z, Wang S-, Kimura T, Ok YS, Yamauchi Y, Chen A-, Wu KC-. *Adv Mater*, 2020, 32: 1907035
21 Lei Q, Guo J, Noureddine A, Wang A, Wuttke S, Brinker CJ, Zhu W. *Adv Funct Mater*, 2020, 30: 1909539
22 Cheng YJ, Hu JJ, Qin SY, Zhang AQ, Zhang XZ. *Biomaterials*, 2020, 232: 119738
23 Li Z, Barnes JC, Bosoy A, Stoddart JF, Zink JI. *Chem Soc Rev*, 2012, 41: 2590–2605
24 Kresge CT, Leonowicz ME, Roth WJ, Vartuli JC, Beck JS. *Nature*, 1992, 359: 710–712
25 Wu SH, Mou CY, Lin HP. *Chem Soc Rev*, 2013, 42: 3862–3875
26 Wan Y, Zhao Y. *Chem Rev*, 2007, 107: 2821–2860
27 Lee JE, Lee N, Kim T, Kim J, Hyeon T. *Acc Chem Res*, 2011, 44: 893–902
28 Slowing I, Trewyn BG, Lin VSY. *J Am Chem Soc*, 2006, 128: 14792–14793
29 Li Z, Yu L, Yang T, Chen Y. *Sci China Chem*, 2018, 61: 1243–1260
30 Kim D, Shin K, Kwon SG, Hyeon T. *Adv Mater*, 2018, 30: 1802309
31 Lin YS, Haynes CL. *J Am Chem Soc*, 2010, 132: 4834–4842
32 Ow H, Larson DR, Srivastava M, Baird BA, Webb WW, Wiesner U. *Nano Lett*, 2005, 5: 113–117
33 Kim J, Lee JE, Lee J, Yu JH, Kim BC, An K, Hwang Y, Shin CH, Park JG, Kim J, Hyeon T. *J Am Chem Soc*, 2006, 128: 688–689
34 Guerrero-Martínez A, Pérez-Juste J, Liz-Marzán LM. *Adv. Mater.*, 2010, 22(11): 1182–1195, doi: 10.1002/adma.200901263
35 Liu J, Liu T, Pan J, Liu S, Lu GQM. *Annu Rev Chem Biomol Eng*, 2018, 9: 389–411
36 Kim J, Kim H , Lee N, Kim T, Kim H, Yu T, Song I , Moon W , Hyeon T. *Angew Chem Int Ed*, 2008, 47: 8438–8441
37 Xu C, Chen F, Valdovinos HF, Jiang D, Goel S, Yu B, Sun H, Barnhart TE, Moon JJ, Cai W. *Biomaterials*, 2018, 165: 56–65

38 Zhang Z, Wang L, Wang J, Jiang X, Li X, Hu Z, Ji Y, Wu X, Chen C. *Adv Mater*, 2012, 24: 1418–1423
39 Liu JN, Bu WB, Shi JL. *Acc Chem Res*, 2015, 48: 1797–1805
40 Lai J, Shah BP, Zhang Y, Yang L, Lee KB. *ACS Nano*, 2015, 9: 5234–5245
41 Liu J, Wang C, Wang X, Wang X, Cheng L, Li Y, Liu Z. *Adv Funct Mater*, 2015, 25: 384–392
42 Liu J, Bu W, Pan L, Shi J. *Angew Chem Int Ed*, 2013, 52: 4375–4379
43 Lin LS, Song J, Song L, Ke K, Liu Y, Zhou Z, Shen Z, Li J, Yang Z, Tang W, Niu G, Yang HH, Chen X. *Angew Chem Int Ed*, 2018, 57: 4902–4906
44 Liu J, Li F, Wang Y, Pan L, Lin P, Zhang B, Zheng Y, Xu Y, Liao H, Ko G, Fei F, Xu C, Du Y, Shin K, Kim D, Jang SS, Chung HJ, Tian H, Wang Q, Guo W, Nam JM, Chen Z, Hyeon T, Ling D. *Nat Nanotechnol*, 2020, 15: 321–330
45 Liu J, Qiao S , Budi Hartono S, Lu G . *Angew Chem Int Ed*, 2010, 49: 4981–4985
46 Li C, Zhang Y, Li Z, Mei E, Lin J, Li F, Chen C, Qing X, Hou L, Xiong L, Hao H, Yang Y, Huang P. *Adv Mater*, 2018, 30: 1706150
47 Zhang Q, Zhang T, Ge J, Yin Y. *Nano Lett*, 2008, 8: 2867–2871
48 Fan W, Shen B, Bu W, Chen F, He Q, Zhao K, Zhang S, Zhou L, Peng W, Xiao Q, Ni D, Liu J, Shi J. *Biomaterials*, 2014, 35: 8992–9002
49 Liu J, Qiao SZ, Chen JS, (David) Lou XW, Xing X, (Max) Lu GQ. *Chem Commun*, 2011, 47: 12578–12591
50 Lee JE, Lee N, Kim H, Kim J, Choi SH, Kim JH, Kim T, Song IC, Park SP, Moon WK, Hyeon T. *J Am Chem Soc*, 2010, 132: 552–557
51 Chen Q, Du Y, Zhang K, Liang Z, Li J, Yu H, Ren R, Feng J, Jin Z, Li F, Sun J, Zhou M, He Q, Sun X, Zhang H, Tian M, Ling D. *ACS Nano*, 2018, 12: 1321–1338
52 Lei Q, Wang SB, Hu JJ, Lin YX, Zhu CH, Rong L, Zhang XZ. *ACS Nano*, 2017, 11: 7201–7214
53 Wu L, Wu M, Zeng Y, Zhang D, Zheng A, Liu X, Liu J. *Nanotechnology*, 2014, 26: 025102
54 Liu R, Zhang Y, Zhao X, Agarwal A, Mueller LJ, Feng P. *J Am Chem Soc*, 2010, 132: 1500–1501
55 Giri S, Trewyn BG, Stellmaker MP, Lin VSY. *Angew Chem Int Ed*, 2005, 44: 5038–5044
56 Kim J, Kim HY, Song SY, Go S, Sohn HS, Baik S, Soh M, Kim K, Kim D, Kim HC, Lee N, Kim BS, Hyeon T. *ACS Nano*, 2019, 13: 3206–3217
57 Wu H, Li F, Wang S, Lu J, Li J, Du Y, Sun X, Chen X, Gao J, Ling D. *Biomaterials*, 2018, 151: 66–77
58 Walther A, Müller AHE. *Chem Rev*, 2013, 113: 5194–5261
59 Li X, Zhou L, Wei Y, El-Toni AM, Zhang F, Zhao D. *J Am Chem Soc*, 2014, 136: 15086–15092
60 Kwon SG, Krylova G, Phillips PJ, Klie RF, Chattopadhyay S, Shibata T, Bunel EE, Liu Y, Prakapenka VB, Lee B, Shevchenko EV. *Nat Mater*, 2015, 14: 215–223
61 Wang Z, Shao D, Chang Z, Lu M, Wang Y, Yue J, Yang D, Li M, Xu Q, Dong W. *ACS Nano*, 2017, 11: 12732–12741
62 Wang Z, Zhang F, Shao D, Chang Z, Wang L, Hu H, Zheng X, Li X, Chen F, Tu Z, Li M, Sun W, Chen L, Dong W-. *Adv Sci*, 2019, 6: 1901690
63 Yang G, Lv R, He F, Qu F, Gai S, Du S, Wei Z, Yang P. *Nanoscale*, 2015, 7: 13747–13758
64 Zhang Z, Liu C, Bai J, Wu C, Xiao Y, Li Y, Zheng J, Yang R, Tan W. *ACS Appl Mater Interfaces*, 2015, 7: 6211–6219
65 Mekaru H, Lu J, Tamanoi F. *Adv Drug Deliver Rev*, 2015, 95: 40–49
66 Gao M, Zeng J, Liang K, Zhao D, Kong B. *Adv Funct Mater*, 2020, 30: 1906950
67 Montalti M, Prodi L, Rampazzo E, Zaccheroni N. *Chem Soc Rev*, 2014, 43: 4243–4268
68 Liu J, Liu Y, Bu W, Bu J, Sun Y, Du J, Shi J. *J Am Chem Soc*, 2014, 136: 9701–9709
69 Wang J, Ma Q, Wang Y, Li Z, Li Z, Yuan Q. *Chem Soc Rev*, 2018, 47: 8766–8803
70 Zou C, Foda MF, Tan X, Shao K, Wu L, Lu Z, Bahlol HS, Han H. *Anal Chem*, 2016, 88: 7395–7403
71 Cheng Y, Jiao X, Fan W, Yang Z, Wen Y, Chen X. *Biomaterials*, 2020, 256: 120191
72 Ni D, Bu W, Ehlerding EB, Cai W, Shi J. *Chem Soc Rev*, 2017, 46: 7438–7468
73 Wang Y, Zheng K, Song S, Fan D, Zhang H, Liu X. *Chem Soc Rev*, 2018, 47: 6473–6485
74 Liu J, Bu J, Bu W, Zhang S, Pan L, Fan W, Chen F, Zhou L, Peng W, Zhao K, Du J, Shi J. *Angew Chem Int Ed*, 2014, 53: 4551–4555
75 Shokeen M, Anderson CJ. *Acc Chem Res*, 2009, 42: 832–841
76 Goel S, Ferreira CA, Chen F, Ellison PA, Siamof CM, Barnhart TE, Cai W. *Adv Mater*, 2018, 30: 1704367
77 Lv R, Yang P, He F, Gai S, Li C, Dai Y, Yang G, Lin J. *ACS Nano*, 2015, 9: 1630–1647
78 Wang Z, Chang Z, Lu M, Shao D, Yue J, Yang D, Zheng X, Li M, He K, Zhang M, Chen L, Dong W. *Biomaterials*, 2018, 154: 147–157
79 Shao D, Li M, Wang Z, Zheng X, Lao YH, Chang Z, Zhang F, Lu M, Yue J, Hu H, Yan H, Chen L, Dong W, Leong KW. *Adv Mater*, 2018, 30: 1801198
80 Yao X, Niu X, Ma K, Huang P, Grothe J, Kaskel S, Zhu Y. *Small*, 2017, 13: 1602225
81 Zhao T, Chen L, Li Q, Li X. *J Mater Chem B*, 2018, 6: 7112–7121
82 Chen W, Cheng CA, Zink JI. *ACS Nano*, 2019, 13: acsnano.8b06655
83 Lee C, Hwang HS, Lee S, Kim B, Kim JO, Oh KT, Lee ES, Choi HG, Youn YS. *Adv Mater*, 2017, 29: 1605563
84 Wu W, Yu L, Jiang Q, Huo M, Lin H, Wang L, Chen Y, Shi J. *J Am Chem Soc*, 2019, 141: 11531–11539
85 Du Y, Yang C, Li F, Liao H, Chen Z, Lin P, Wang N, Zhou Y, Lee JY, Ding Q, Ling D. *Small*, 2020, 16: 2002537
86 Mellman I, Coukos G, Dranoff G. *Nature*, 2011, 480: 480–489
87 Singha S, Shao K, Ellestad KK, Yang Y, Santamaria P. *ACS Nano*, 2018, 12: 10621–10635
88 Ding B, Shao S, Yu C, Teng B, Wang M, Cheng Z, Wong K-, Ma P, Lin J. *Adv Mater*, 2018, 30: 1802479
89 Müller LK, Simon J, Rosenauer C, Mailänder V, Morsbach S, Landfester K. *Biomacromolecules*, 2018, 19: 374–385
90 Chen Y, Chen H, Shi J. *Adv Mater*, 2013, 25: 3144–3176